Mechanisms of Global Teleconnections Associated with the Asian Summer Monsoon: An Intermediate Model Analysis*

FEI LIU

International Pacific Research Center, University of Hawaii at Manoa, Honolulu, Hawaii

BIN WANG

International Pacific Research Center and Department of Meteorology, University of Hawaii at Manoa, Honolulu, Hawaii

(Manuscript received 1 May 2012, in final form 7 September 2012)

ABSTRACT

The Indian summer monsoon (ISM) and western North Pacific summer monsoon (WNPSM) are two subsystems of the Asian summer monsoon, and they exhibit different global teleconnection patterns. The enhanced ISM strengthens the South Asian high and Mascarene high, and the WNPSM excites a meridional tripolar wave train in the Northern Hemisphere and affects the Australian high in the Southern Hemisphere. To understand the dynamics behind these global teleconnections, especially the processes responsible for the cross-equatorial teleconnection, an intermediate model, describing a two-level troposphere and a steady planetary boundary layer (PBL), is linearized from the background horizontal wind field. The model results indicate that the ISM heating, located under the strong easterly vertical shear (VS) and close to the westerly jet in the Northern Hemisphere, can excite a barotropic Rossby wave that emanates northwestward and then propagates downstream along the westerly jet. Since the WNPSM heating is far away from the westerly jet over the North Pacific, it only excites a weak Rossby wave train, which cannot explain the meridional tripolar teleconnection associated with the WNPSM. It is found that both the ISM and WNPSM heating excite strong teleconnections in the Southern Hemisphere via an advection mechanism; that is, the background upper-level northerly winds can transport energy across the equator from the Northern Hemisphere summer monsoon to the Southern Hemisphere westerly jet. In addition, the PBL enhances monsoon teleconnections by trapping more energy in the upper troposphere. The elevated maximum monsoon heating also reinforces upper-level perturbations and enhances the teleconnection pattern.

1. Introduction

The Asian summer monsoon (ASM) variability has a global impact on the Northern Hemisphere circulation (Nitta 1987; Hoskins and Rodwell 1995; Rodwell and Hoskins 1996; Kripalani et al. 1997; Wang et al. 2001; Ding and Wang 2005, 2007; Lin 2009), as well as on the Southern Hemisphere circulation (Nitta 1989; Wang et al. 2001; Lin 2009). The ASM consists of two subsystems: the Indian summer monsoon (ISM) and the western North Pacific summer monsoon (WNPSM) (Wang and Fan 1999; Wang et al. 2001), which are associated with the strong convection centered over the Bay of Bengal (Fig. 1a) and the South China Sea/Philippine Sea, respectively (Fig. 1b). These two subsystems have distinct teleconnection patterns (Wang et al. 2001). The strong ISM excites an enhanced upper-level Tibetan Plateau high and Mascarene high (Fig. 1a), and the strong WNPSM excites a meridional tripolar wave train in the Northern Hemisphere and an upper-level Australian high (Fig. 1b). It is not clear why these two subsystems have such different teleconnection patterns. In addition, it is necessary to find out why the ASM heating in the Northern Hemisphere can produce a Rossby wave source in the Southern Hemisphere that is far away from the monsoon region.

* School of Ocean and Earth Science and Technology Contribution Number 8748 and International Pacific Research Center Publication Number 914.

Corresponding author address: Dr. Bin Wang, IPRC and Department of Meteorology, University of Hawaii at Manoa, 401 Post Bldg., 1680 East–West Road, Honolulu, HI 96822.
E-mail: wangbin@hawaii.edu

DOI: 10.1175/JCLI-D-12-00243.1

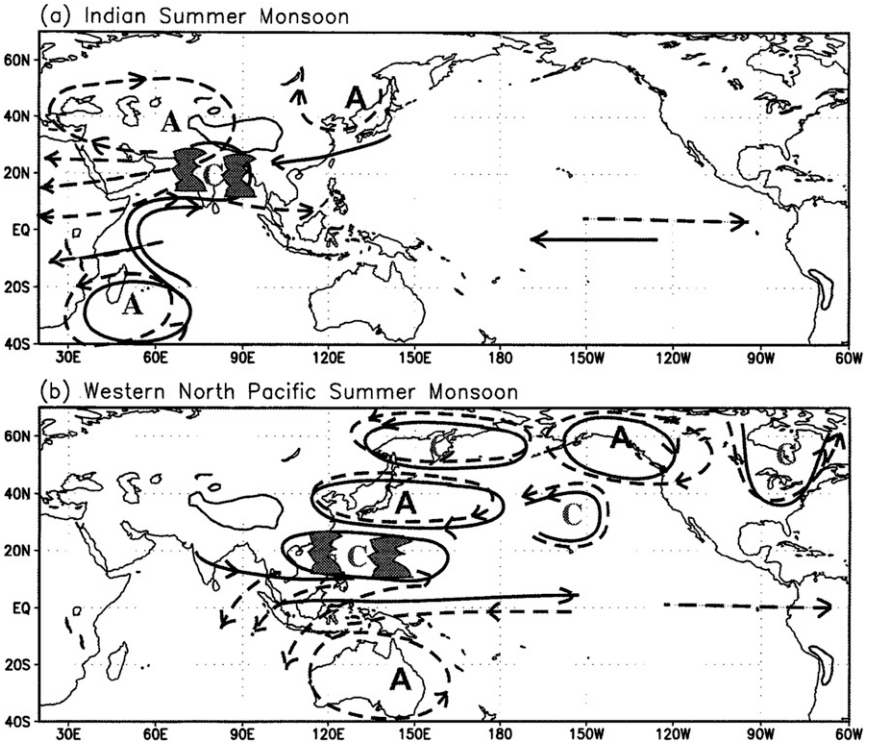

FIG. 1. Schematic diagrams showing the major circulation anomalies associated with (a) a strong ISM and (b) a strong WNPSM. The lower-level and upper-level circulation anomalies are denoted by solid and dashed lines, respectively; the letters A and C represent anticyclone and cyclone, respectively. [Adapted from Wang et al. (2001).]

The tropical deep convective heating excites baroclinic Matsuno–Gill patterns that are trapped near the equator (Matsuno 1966; Gill 1980; Geisler 1981; Geisler and Stevens 1982; Silva Dias et al. 1983; Fulton and Schubert 1985; Davey and Gill 1987; Lee et al. 2009). The off-equatorial monsoon heating also excites equatorially asymmetric baroclinic Matsuno–Gill patterns that have strong cyclones near and to the west of the heating (Gill 1980). Since the ASM heating is located under the strong upper-level easterly, in order for an equatorial heating to build its extratropical teleconnection, barotropic modes must be excited (Wang and Xie 1996; Lee et al. 2009). The vertical shear (VS) of mean winds is one of the mechanisms for generation of barotropic modes (Webster 1981, 1982; Lim and Chang 1983, 1986; Kasahara and da Silva Dias 1986; Wang and Xie 1996; Majda and Biello 2003; Lee et al. 2009). In addition, Sardeshmukh and Hoskins (1988) proposed that the equatorial forcing in easterly winds can lead to a Rossby wave source in the subtropical westerlies.

In addition to the VS of mean winds, the planetary boundary layer (PBL) can also produce a barotropic mode (Lim and Chang 1983, 1986). However, their works were based on an *f*-plane model, in which motions are assumed to be meridionally invariable, so that neither equatorial waves nor midlatitude Rossby waves exist. The role of the PBL in the teleconnection associated with the ASM remains elusive.

The vertical heating distribution (VHD) associated with the tropical convection also affects the simulation of the extratropical teleconnection. Some models can simulate the convective responses to the tropical sea surface forcing, while these models can have poor performance in predicting extratropical responses. The paradox is attributable to the incorrect simulation of the vertical profile of the tropical convective heating (Michaels 2005). The VHD seems to be fundamental in affecting the structure of forced responses. The deep convection associated with larger equivalent depth can enforce teleconnection far away from the forcing and excite stronger extratropical responses than the shallow heating (Ting and Sardeshmukh 1993; Wu et al. 2000). So it is interesting to discuss the role of the VHD in the teleconnection of the ASM.

Wang and Xie (1996) extended Matsuno's theory on equatorial waves by including the effects of background

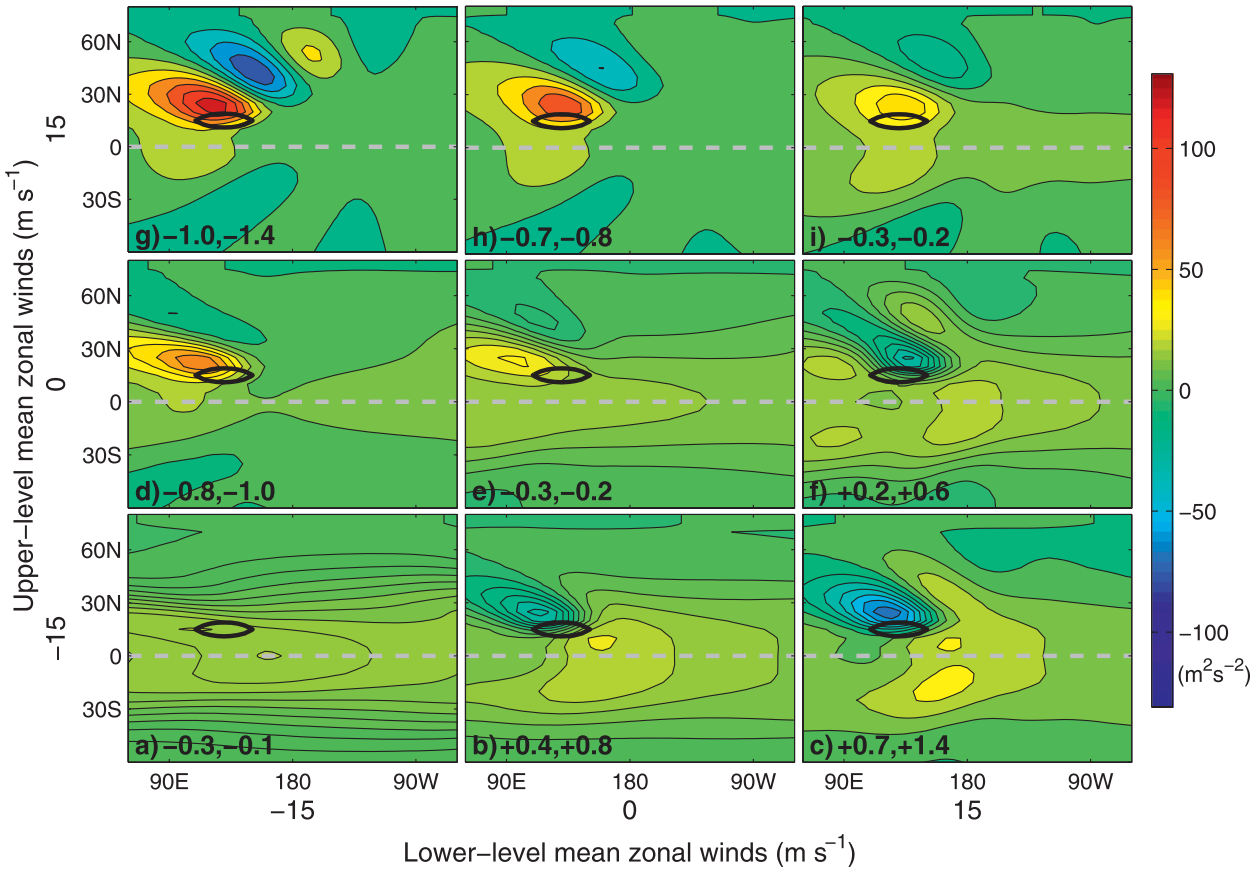

FIG. 2. Role of VS in coupling the baroclinic and barotropic modes. The contours denote barotropic geopotential anomalies excited by the same heating (black circle centered at 15°N, 130°E) under nine sets of different horizontally uniform background zonal winds. (bottom right to top left) An easterly VS changes to a westerly VS; (bottom left to top right) barotropic easterly winds changes to westerly winds; and (a),(e),(i) there is no VS in. The two numbers in each panel represent the "conversion ratio" from baroclinic to barotropic modes for the geopotential and vorticity perturbations, respectively.

mean flows. They found that the vertical wind shear can drastically change the Rossby wave response because it can couple the heat-induced baroclinic motion with barotropic wave motion, generating a barotropic response that establishes a tropical–extratropical teleconnection even in the presence of equatorial upper-level easterlies. On the other hand, the baroclinic component of Rossby wave remains trapped near the equator, but the Rossby waves have enhanced amplitudes in the lower (upper) troposphere under easterly (westerly) VS. This explains why Rossby waves are most unstable in the monsoon regions where easterly VS prevails.

In this work, we extend the Gill model in a similar matter. The two-level model of Wang and Xie (1997) and Wang (2000) has been used, but we add a steady PBL and also make the level depths variable to mimic different VHD. This intermediate model enables us to study the effects of the VS and PBL as well as the VHD on heating-induced circulations. Therefore, the present intermediate model provides a simple yet useful tool to study global atmospheric responses to the imposed tropical heat forcing.

The intermediate model is summarized in section 2, and section 3 presents the role of the VS, PBL, and VHD in coupling the baroclinic and barotropic modes. The global teleconnections of the ASM are discussed in section 4. This paper ends with a discussion in section 5.

2. Intermediate model

a. Model equations

The model used here is an extension of the model for studying the low-frequency equatorial waves in the mean winds developed by Wang and Xie (1997) and Wang (2000), and it can also be seen as an extension of the Gill model (Gill 1980) or its generalization (Zhang and Krishnamurti 1996) by including a PBL and variable elevation of the maximum heating. Details of the two-level model for the free troposphere are described

TABLE 1. Major parameter values used in the intermediate model.

Variable	Description	Value
Δp_b	Depth of PBL	~100 hPa
$\Delta p_1, \Delta p_2$	Depth of upper and lower troposphere	~400 hPa
p_m	Height where the heating occurs	~500 hPa
ε_e	Equatorial momentum damping	0.58×10^{-5} s^{-1} (2 day)$^{-1}$
μ	Newtonian cooling coefficient	0.58×10^{-5} s^{-1} (2 day)$^{-1}$
E_λ	Momentum damping of PBL	3.0×10^{-5} s^{-1}
K	Horizontal diffusion coefficient	5×10^5 m^2 s^{-1}
$S(p)$	Mean static stability parameter at the middle level	3×10^{-6} m^2 s^{-2} Pa^{-2}
R	Gas constant of air	287 J kg^{-1} °C^{-1}
C_p	Specific heat at constant pressure	1004 J kg^{-1} °C^{-1}

in appendix A, and the PBL model is presented in appendix B. Equations (A2) and (A3) are not self-contained because the geopotential perturbation relies on arbitrary references. To solve this problem, many works studied the vorticity equation by neglecting the barotropic divergence. Here we add a barotropic PBL equation [Eq. (B2)] to predict the geopotential perturbation of the PBL, which is assumed to be equal to that of the lower level.

b. Model limitations

This paper only discusses the linear processes relevant to the teleconnections of the ASM. The nonlinear processes between the perturbations and mean states need to be explored in the future works. Meanwhile, the flat lower-boundary condition used in this intermediate model neglects the topographic effects that influence the low-level monsoon inflow, and the blocking effect of the mountains on both the summer low-latitude easterlies and midlatitude westerlies are important (Rodwell and Hoskins 2001).

c. Numerical schemes

Equations (A2), (A3), (B2), and (B4) form a complete intermediate model, which includes a generation of a baroclinic mode by heating, a coupling of barotropic and baroclinic modes by the VS, and a transport of energy by mean winds. Roles of the PBL and VHD

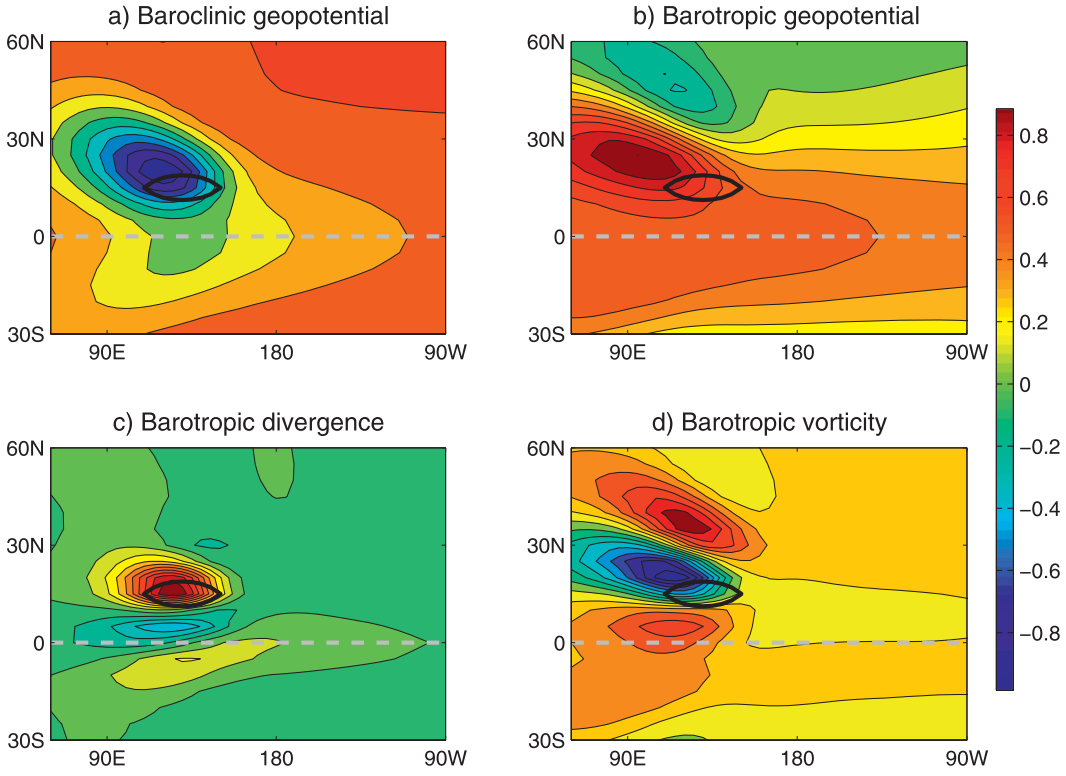

FIG. 3. PBL-induced barotropic responses excited by the heat forcing (black circle) without mean winds. Contours are drawn for (a) baroclinic geopotential, (b) barotropic geopotential, (c) barotropic divergence, and (d) barotropic vorticity, which are normalized with respect to their magnitudes of 106 m^2 s^{-2}, 31 m^2 s^{-2}, 1.1×10^{-7} s^{-1}, and 4.5×10^{-7} s^{-1}, respectively.

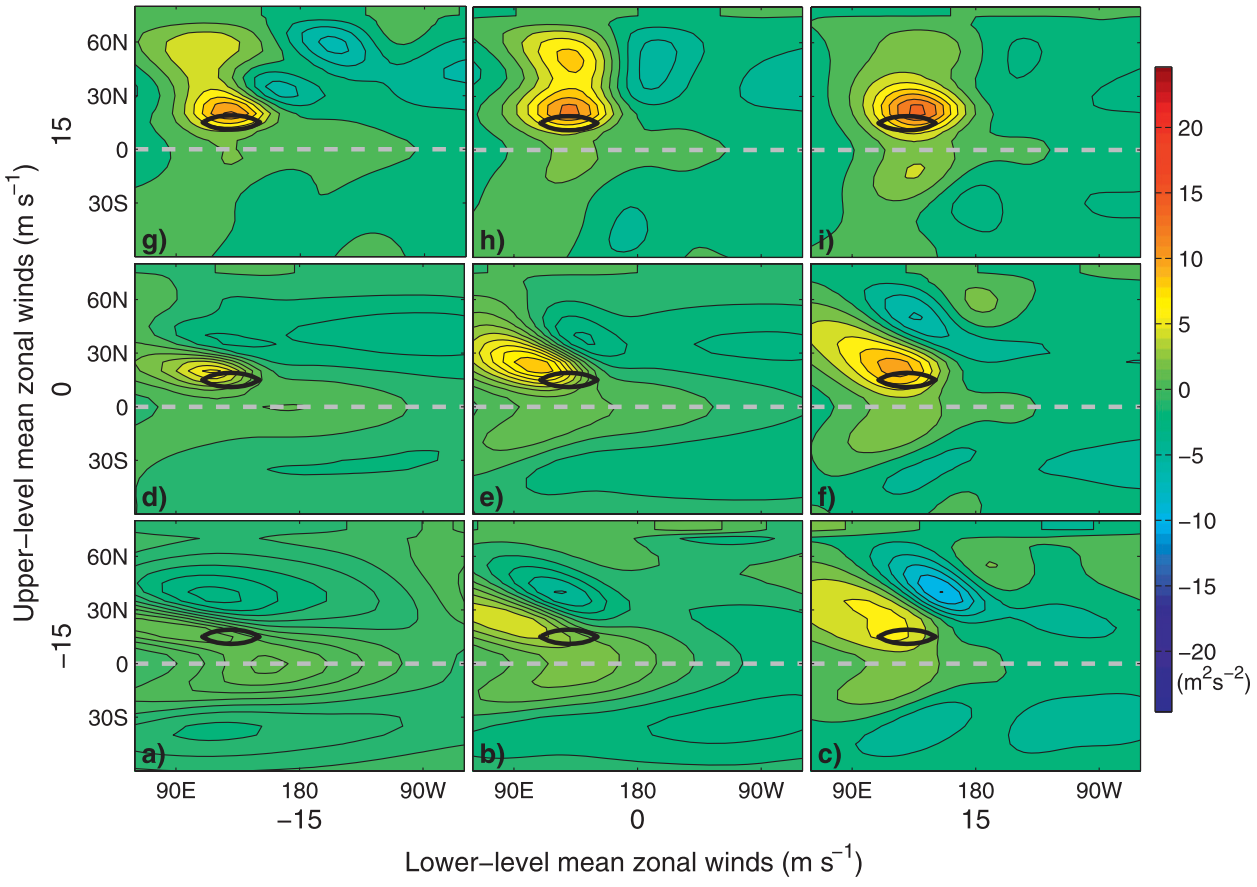

FIG. 4. Role of the PBL in coupling the baroclinic and barotropic modes. As in Fig. 2, except that the contours denote the barotropic geopotential differences between the sensitivity experiment with a PBL pressure depth of 150 hPa and the control experiment with an original PBL depth of 100 hPa.

have also been included. This model is written in spherical coordinates and can be solved as an initial value problem. The finite difference method is adopted in both time and space. The time integration scheme is centrally differenced with a time step of 2.5 min and a time-average coefficient of 0.125. For instance, on step n, any variable A_n can be calculated by $A_n = A_n^* + 0.125(A_{n+1}^* + A_{n-1} - 2A_n^*)$, where the subscript denotes the step number. Here A_n^* and A_{n+1}^* are calculated from A_{n-1} by the forward difference method. The spatial resolution is 2.5° longitude by 2.5° latitude, and the model domain is from 82.5°S to 82.5°N. To calculate the geopotential perturbation of the PBL, the shooting method (Langer 1960, 243–255) is applied to solve the elliptic equations [see Eq. (B2)] at every calculation step. Sensitivity tests were performed by using some coarse spatial grid sizes and show that the results are not sensitive to the horizontal resolution.

The zonal boundary condition is periodic around the globe, and the fluxes of mass, momentum, and heat normal to the lateral boundary vanish. This lateral boundary condition cuts off the energy path to the polar region. For instance, in a solid-body rotation background flow, the forced response reaches only a half of the great circle (Fig. 2i), whereas with the meridional periodic condition the whole great circle is produced (Longuet-Higgins 1964). In the present work, we focus on the teleconnection of the ASM, during which the mean westerly jet, acting as a waveguide (Branstator 2002) in the midlatitude, tends to trap Rossby waves in it. So the no-flux lateral boundary condition has a relatively small impact on the teleconnection associated with the ASM.

In the present model, the monsoon internal heating at the middle troposphere takes the form of

$$Q = Q_0 \exp\left[-\left(\frac{x - x_0}{L_{xx}}\right)^2\right] \exp\left[-\left(\frac{y - y_0}{L_{yy}}\right)^2\right]. \quad (1)$$

Unless otherwise mentioned, $Q_0 = 2.5$°C day^{-1}, $x_0 = 130$°E, $y_0 = 15$°N, $L_{xx} = 25$°, and $L_{yy} = 5$°. (The above

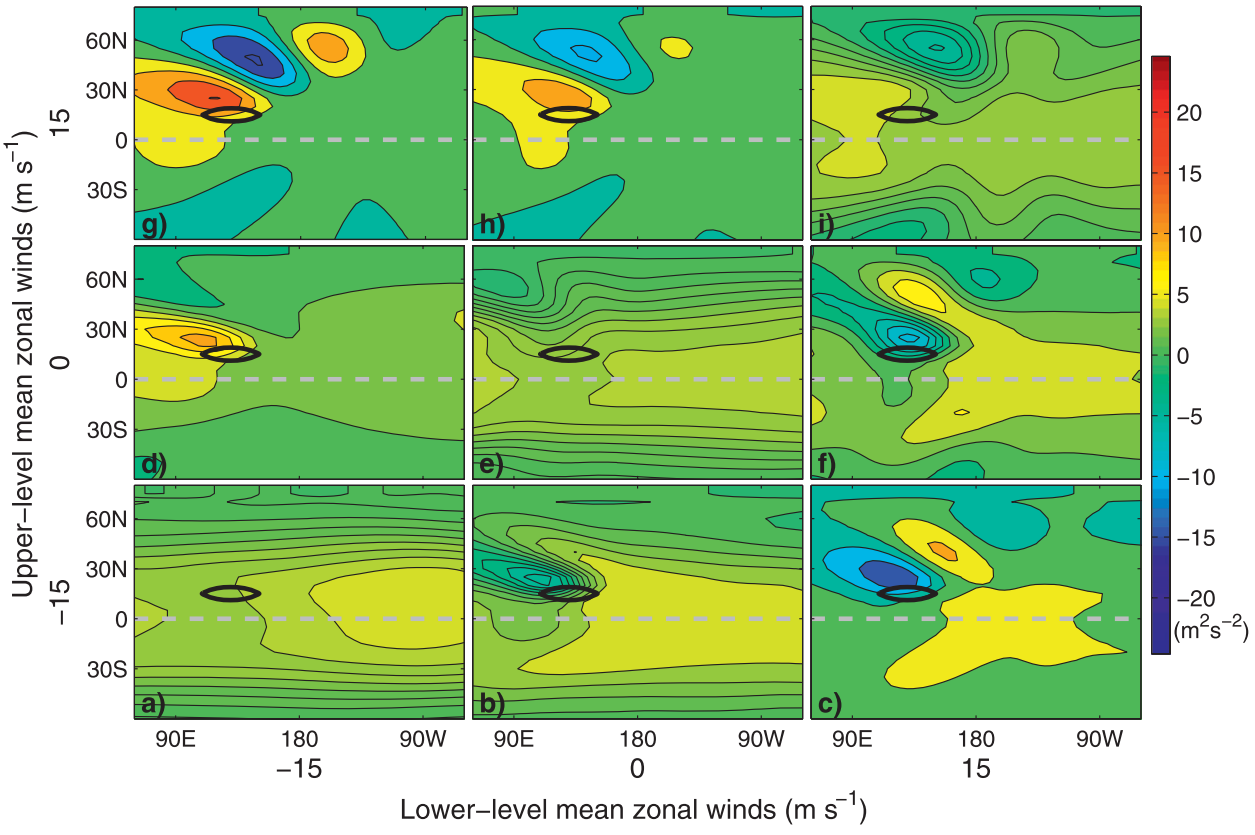

FIG. 5. Role of the VHD in coupling the baroclinic and barotropic modes. As in Fig. 2, except that contours denote the barotropic geopotential differences between the sensitivity experiment with a higher heating at 400 hPa and the control experiment with an original heating at 500 hPa.

heating is used in Figs. 2, 3, 4, 5, and 11 for the idealized experiments. However, for the ISM heating, $x_0 = 87°$E, $y_0 = 18°$N, and $L_{xx} = 15°$, and for the WNPSM heating, $x_0 = 135°$E and $y_0 = 15°$N were used in Figs. 8, 9, 10, 12, and 13.) Sensitivity experiments show that the heating structure does not affect the result qualitatively. The strength of the heat forcing only affects the amplitude of the responses, and a slight change of the heating location does not produce significant differences in responses. The model parameters are listed in Table 1. In the following experiments, the model output on day 40 is studied, when the model reaches a steady state.

3. Role of the VS, PBL, and VHD in coupling the baroclinic and barotropic modes

a. Role of the VS

To study the role of the VS, the same heating is located under nine sets of different horizontally uniform mean zonal winds (Fig. 2), where the easterly VS changes to westerly VS from the bottom-right to top-left panels, the barotropic easterly changes to westerly from the bottom-left to top-right panels, and the VS vanishes in Figs. 2a,e,i. To represent the efficiency of the conversion from the baroclinic to barotropic mode, a "conversion ratio" is defined by the maximum amplitude of the barotropic versus baroclinic mode in perturbation geopotential (ϕ_+/ϕ_-) or vorticity (ζ_+/ζ_-). A large absolute value of the ratio means an efficient conversion from the baroclinic to barotropic mode. A positive (negative) ratio represents that the barotropic mode is in (out of) phase with the baroclinic mode, and correspondingly the energy will be trapped in the lower (upper) troposphere according to Eq. (A4).

The VS does yield significant barotropic modes (Fig. 2), and the off-equatorial heating produces results similar to those of the equatorially symmetric heating (Wang and Xie 1996; Lee et al. 2009). These results are as follows: 1) The generating efficiency of barotropic modes increases with strong VS, represented by the large conversion ratio of geopotential or vorticity (Figs. 2c,g). 2) The westerly VS traps the energy in the upper

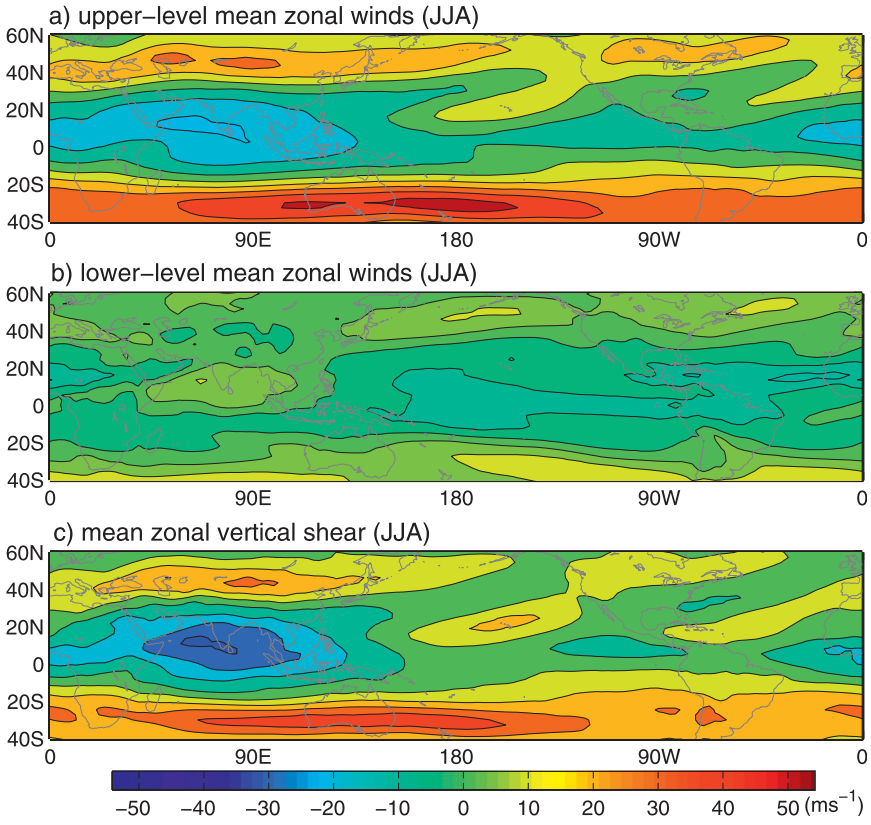

FIG. 6. Observed climatological mean (a) upper-level (200 hPa) zonal winds, (b) lower-level (700 hPa) zonal winds, and (c) mean vertical shear of zonal winds during June–August (JJA).

troposphere, represented by the negative conversion ratios of geopotential perturbations from baroclinic to barotropic mode (Figs. 2d,g,h), while the easterly VS traps the energy in the lower troposphere (Figs. 2b,c,f), confirming the theory of Wang and Xie (1996). 3) The VS favors coupling the vorticity, represented by the large conversion ratios of vorticity (Figs. 2c,g). 4) The mean barotropic westerly winds are favorable for the teleconnection (Fig. 2h), while the easterly winds play a destructive role in the teleconnection (Fig. 2b), confirming the previous results (Hoskins and Karoly 1981; Lee et al. 2009). 5) The barotropic mode excited by the easterly VS can also propagate to high latitudes under the mean barotropic westerly winds (Fig. 2f), which helps to explain how the monsoon heating produces its global teleconnection.

b. Role of the PBL

Because of the inclusion of the PBL, this model can produce a barotropic mode without the VS (Fig. 2e). This barotropic response features a strong cyclone extending to the midlatitude, and its magnitude reaches 30% of the baroclinic mode. The barotropic mode is forced by the PBL divergence/Ekman pumping, whose structure is assumed to be the same but out of phase with that of the barotropic divergence. Usually, the barotropic divergence is trapped near the heat forcing (Fig. 3c). Because of the increase of the Coriolis parameter with latitude, considerable barotropic vorticity is generated in the extratropics, forming a wave pattern that propagates poleward (Fig. 3d). The coincidence of the extratropical barotropic vorticity (Fig. 3d) and geopotential (Fig. 3b) perturbations reflects the dominant role of geostrophic vorticity balance in the extratropical responses.

Without mean winds, Figs. 3a and 3b show that the PBL produces out-of-phase barotropic mode with baroclinic mode, which means that the energy is trapped in the upper troposphere, as happens with the mean westerly VS (Fig. 2g). Meanwhile, the barotropic mode forced by the PBL can also propagate to high latitudes under the mean barotropic westerly winds (Fig. 2i).

The role of the PBL in coupling the barotropic and baroclinic modes can be represented by a sensitivity experiment with a deep PBL pressure depth of 150 hPa

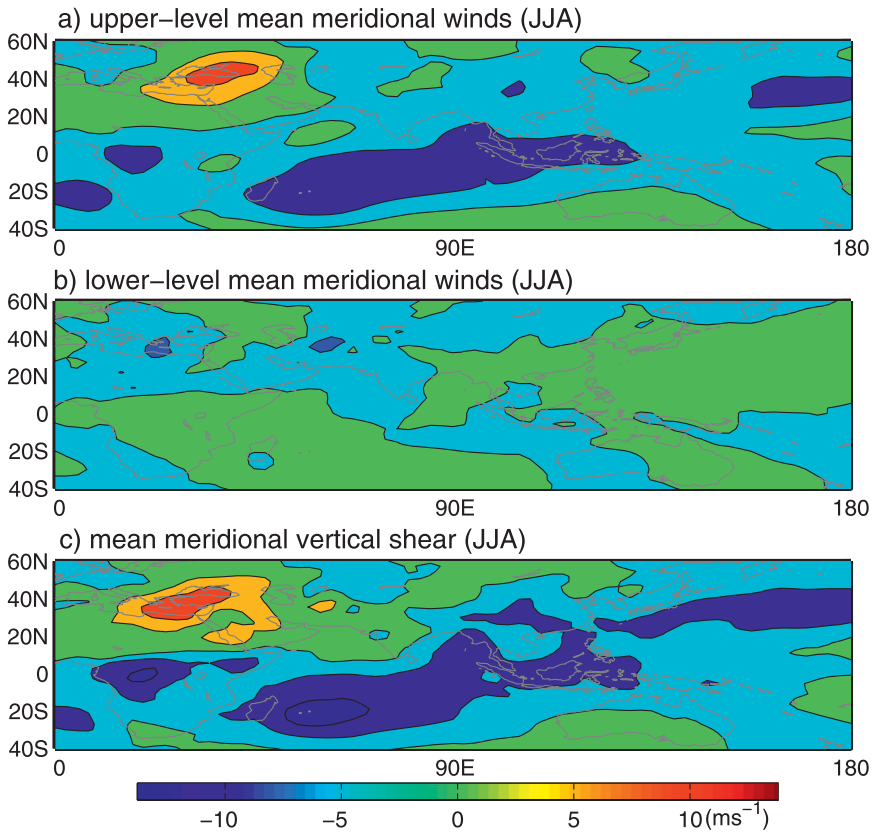

FIG. 7. As in Fig. 6, but for the mean meridional winds.

(Fig. 4). Compared to Fig. 2, without VS or with westerly VS, a deep PBL enhances the barotropic response near the heating (Fig. 4). Because the PBL produces an out-of-phase barotropic response with that excited by the easterly VS (Figs. 2c and 3b), the deep PBL weakens the negative barotropic responses near the heating under the easterly VS (Figs. 4b,c,f). By Eq. (A4), the PBL always enhances the upper-level disturbances regardless of the background VS (not shown). Furthermore, the mean westerly winds that are important for the teleconnection prevail in the upper troposphere, and thus the enhanced upper-level disturbances associated with the PBL effect should have a strong teleconnection in the mean westerly winds.

c. *Role of the VHD*

The depth variation of this intermediate model allows us to study the role of the VHD in extratropical responses. The same experiments as in Fig. 2 are run, except that the heating is located at a high height of 400 hPa. Compared to Fig. 2, Fig. 5 exhibits that the elevation of the heat forcing will enhance the barotropic mode for all different VS. Although the lower-level perturbations have been suppressed (not shown), the upper-level perturbations are enhanced, so the global teleconnection in the upper-level mean westerly winds is also enhanced accordingly.

4. Teleconnection patterns associated with the ASM

The observed monthly mean background winds are obtained from the National Centers for Environmental Prediction (NCEP)–National Center for Atmospheric Research (NCAR) global reanalysis (Kalnay et al. 1996). During the boreal summertime, the summer westerly jet along 40°N is relatively weak and far away from the equator in the Northern Hemisphere, but the strong winter westerly jet is close to the equator in the Southern Hemisphere (Fig. 6a). The strong upper-level easterly winds prevail over the tropical regions and produce strong easterly VS there (Fig. 6c). Compared to the mean zonal winds, the mean meridional winds are relatively weak, with amplitude only about one-fifth of that of the mean zonal winds (Fig. 7). In the tropics, northerly winds prevail in the upper level (Fig. 7a), and southerly winds exist in the lower level (Fig. 7b).

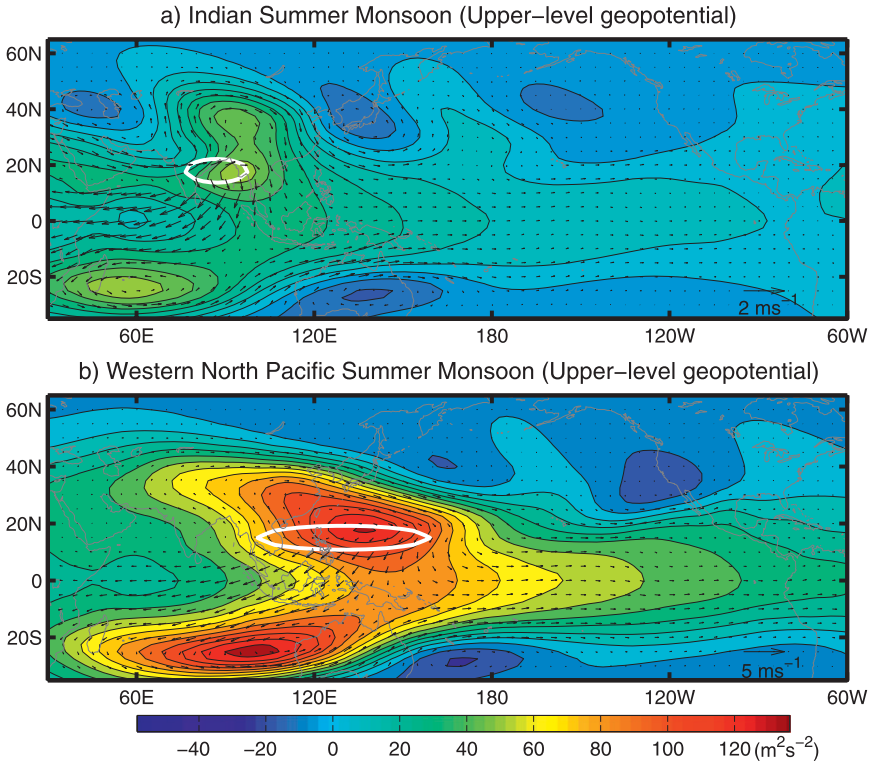

FIG. 8. Simulated global teleconnection associated with (a) the ISM and (b) the WNPSM. Upper-level geopotential anomalies (contours) are excited by the monsoon heat forcing (white circle) under the observed JJA mean winds.

In this intermediate model, to mimic the observed heating structures and amplitudes (Fig. 1), a WNPSM heating with a standard structure and an ISM heating with a smaller zonal scale of $L_{xx} = 15°$ are placed at the same locations as in Figs. 1b,a, respectively. The observed seasonal mean winds (Figs. 6 and 7) are used as the mean state, and the maximum heating is put at 500 hPa.

a. Teleconnection in the Northern Hemisphere

The upper-level circulations associated with the ASM are presented in Fig. 8. The ISM heating excites a very similar response with the observation (Fig. 1a), and a zonally oriented wave train appears in the Northern Hemisphere (Fig. 8a). Probably because of the lack of the topography, the simulated Tibetan Plateau high shifts eastward compared to the observation (Fig. 1a).

To understand the dynamics of the teleconnection associated with the ISM heating, we studied the responses of two different vertical modes. Since the baroclinic mode is trapped near the heating (Fig. 9a), the extratropical teleconnection mainly comes from the barotropic mode (Fig. 9b). Under the strong easterly VS, the ISM heating excites strong barotropic Rossby wave that emanates northwestward (Figs. 2c and 9b), which dissipates during the emanation without the role of mean westerly winds (Fig. 2c). In boreal summer, the westerly jet prevails along 40°N (Fig. 6a), so the Rossby wave can grow and propagate downstream (Branstator 1983, 2002; Hoskins and Ambrizzi 1993). This result shows that the ISM heating does contribute to the boreal summer circumglobal teleconnection found by Ding and Wang (2005, 2007).

Different from the ISM, the WNPSM has an impact on the western coast of North America, while the teleconnection in the Northern Hemisphere is weak (Fig. 8b), because the WNPSM heating is too far away from the background westerly jet. Lee et al. (2009) also showed that the heat forcing associated with the ENSO has weak teleconnection when it is far away from the westerly jet. In observation, the cooling associated with the WNPSM is located at the midlatitudes and has a smaller amplitude compared to the heating (Fig. 9a of Wang et al. 2001). We assume that the cooling has the same structure as in Eq. (1), except that $x_0 = 130°\text{E}$, $y_0 = 35°\text{N}$, and $Q_0 = 2.5/4$ (°C day^{-1}).

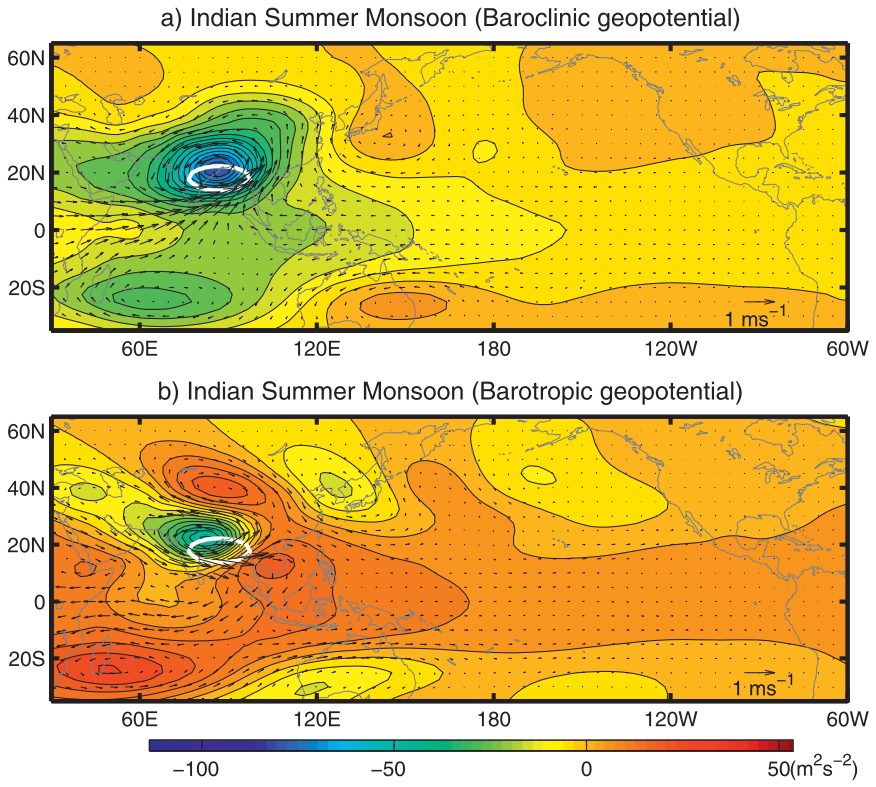

FIG. 9. As in Fig. 8a, but for (a) the baroclinic and (b) the barotropic modes of the ISM.

In this intermediate model, when the midlatitude cooling associated with the WNPSM is included, our experiments show that it can excite a anticyclonic response in the lower troposphere (Fig. 10b) that is consistent with the observation (Fig. 1b). However, in the upper troposphere, the simulated midlatitude cyclone (Fig. 10a) is inconsistent with the observed anticyclone (Fig. 1b). There have other potential factors for influencing the teleconnection pattern, such as the Tibetan Plateau effect that was missed in the model. Further investigation is required for explanation of the meridional barotropic teleconnection associated with the WNPSM.

b. Teleconnection in the Southern Hemisphere

The ASM heating also excites strong responses in the Southern Hemisphere (Fig. 8). Like in the observation (Fig. 1a), the ISM heating produces a strong Mascarene high (Fig. 8a), and the WNPSM heating excites an Australian high, although the location is shifted to the west of Australia (Fig. 8b). Since the ASM heating is far away from the westerly jet of the Southern Hemisphere, the teleconnection in the Southern Hemisphere should be very weak (Lee et al. 2009). This is also shown in Fig. 2; for example, the disturbances are mainly trapped near the heating in the Northern Hemisphere. Thus, to have a strong teleconnection in the Southern Hemisphere, there must be a bridge that transfers the energy across the equatorial region against strong cumulus friction (Lin et al. 2008).

During boreal summer, obvious meridional VS occurs in the equatorial region (Fig. 7c), where southerly winds exist in the lower level (Fig. 7b), while northerly winds prevail in the upper level (Fig. 7a). We recall the patterns induced by the same heating under different horizontally uniform mean zonal winds (Fig. 2), which cannot explain the Southern Hemisphere responses at all. Now we add in the mean wind field, additional horizontally uniform mean meridional winds of -5 and $+5$ m s^{-1} at the upper and lower level, respectively. The results are shown in Fig. 11. Compared to Fig. 2, the basic-state meridional winds do enhance the perturbations in the Southern Hemisphere, no matter whether under the westerly VS or easterly VS. After removing the lower-level mean meridional winds, results similar to Fig. 11 are obtained, while the lack of the upper-level mean meridional winds produces very weak perturbations in the Southern Hemisphere and presents similar patterns to Fig. 2. These results reveal that the upper-level

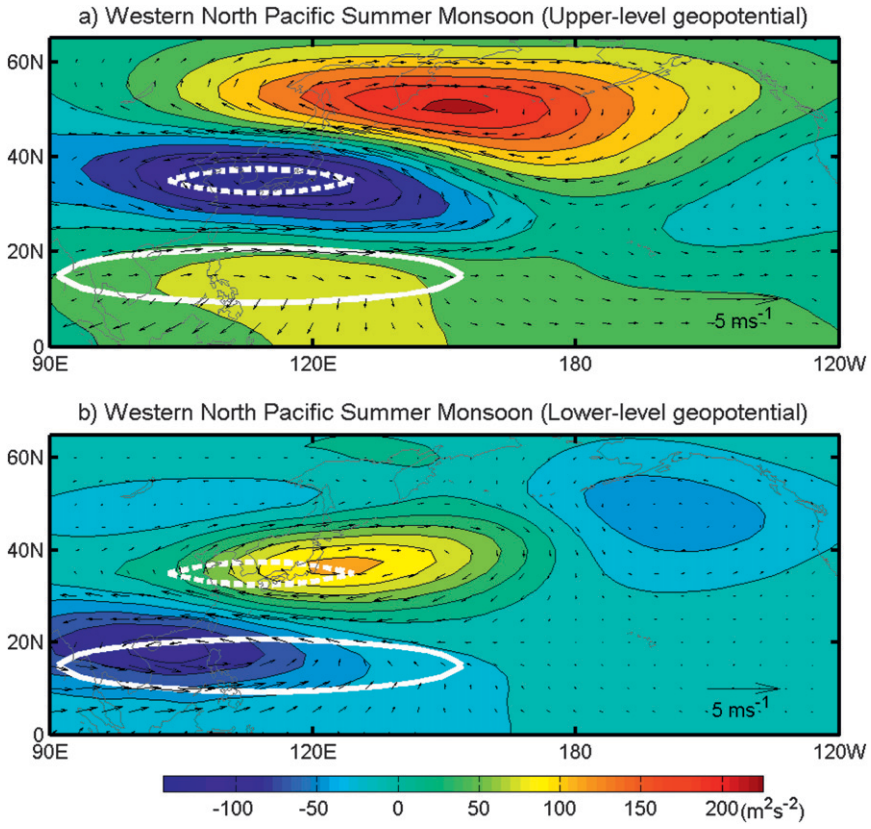

FIG. 10. Intermediate model-simulated meridional tripolar vortices associated with the WNPSM. The positive (negative) monsoon heating is denoted by the solid (dashed) white circle.

northerly winds play a critical role in advection of the energy from the top of the monsoon heating to the Southern Hemisphere and in producing a strong teleconnection there.

To confirm this assertion, a sensitivity experiment in which meridional mean flows are excluded has been run, and the results are shown in Fig. 12. Without the mean meridional winds, both the ISM and WNPSM heating excite strong teleconnection patterns in the Northern Hemisphere (Fig. 12), but the Mascarene and Australian highs are too weak compared to Fig. 8. This result is consistent with the work of Lin (2009), in which he included the mean meridional winds and simulated strong Southern Hemisphere teleconnections associated with the ISM and WNPSM in a linear general climate model. For the WNPSM, because of the lack of the advection role of the mean meridional winds, the energy is trapped in the Northern Hemisphere, which can propagate to high latitudes in the mean westerly winds over the North Pacific and form a strong response there (Fig. 12b).

5. Summary and discussion

The global teleconnections associated with two different Asian summer monsoon (ASM) subsystems, the Indian summer monsoon (ISM) and the western North Pacific summer monsoon (WNPSM), are found to be controlled by the mean-state winds. The ISM, characterized by major convection centered over the Bay of Bengal, is located under the strong easterly vertical shear (VS) (Figs. 1a and 6c). Through the coupling effect of this easterly VS the barotropic mode can be effectively excited, which tends to emanate northwestward (Fig. 2c). Since the ISM is close to the boreal summer westerly jet located near 40°N, the Rossby wave response can propagate downstream in the westerly jet (Figs. 8a and 9b). This means that the ISM does have important impacts on the circumglobal teleconnection as detected by Ding and Wang (2005, 2007).

The WNPSM, characterized by a major convection centered over the Philippine Sea, is also located under the easterly VS, but far away from the summer westerly jet, so the WNPSM heating only generates

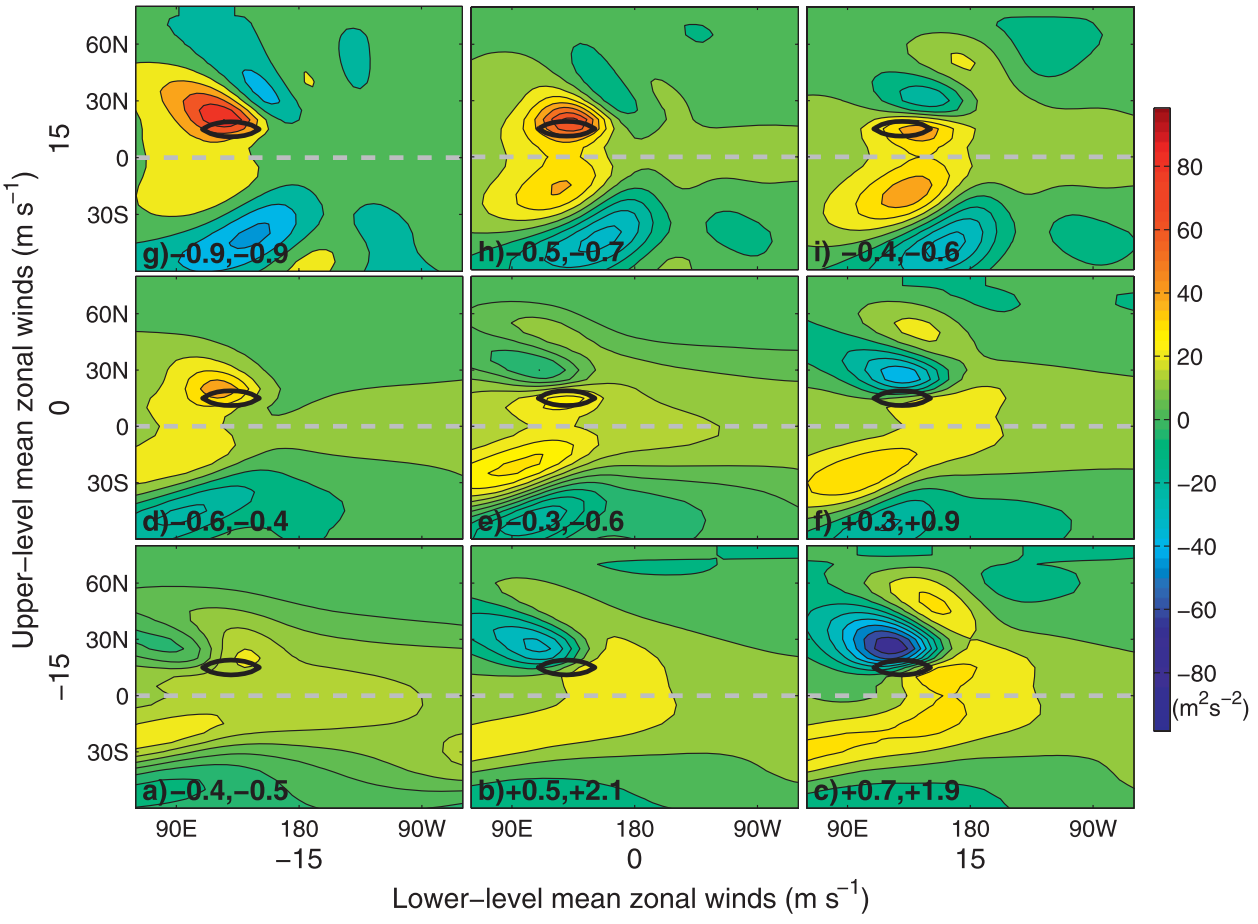

FIG. 11. As in Fig. 2, but with the horizontally uniform mean meridional winds (+5 m s^{-1} in the lower level and −5 m s^{-1} in the upper level) included.

a weak teleconnection in the Northern Hemisphere (Fig. 8b) and cannot fully explain the meridional tripolar teleconnection pattern detected in observations (Fig. 1b).

Although far away from the Southern Hemisphere, the ASM produces a strong teleconnection in the Southern Hemisphere and affects the Mascarene and Australia highs (Wang et al. 2001). The upper-level northerly winds have been demonstrated to play a critical role in transporting energy from the ASM region across the equator and producing strong responses in the westerly jet of the Southern Hemisphere.

In addition to the VS, the planetary boundary layer (PBL) also provides a process to couple the barotropic and baroclinic modes (Figs. 3 and 4). To quantify the role of the PBL and vertical heating distribution (VHD), we compare the control experiment with a sensitivity experiment SE1 in which the PBL pressure depth is deeper (150 hPa), and with a sensitivity experiment SE2 in which the heating is higher (at 400 hPa). A ratio δ is defined as the maximum geopotential amplitude of SE1 (or SE2) versus that of the corresponding control experiment with a PBL depth of 100 hPa and a heating at 500 hPa. The increase in the ratio, $\delta - 1$, can be used to quantify the effect of the PBL depth (or elevated heating). To represent the roles of the PBL (or VHD) near and away from the monsoon heating, respectively, we further separate it into a local part and a teleconnection part, which are calculated from the amplitude ratio within or out of the circle that has a diameter of 20° longitude centered on the heat forcing. Although the PBL produces an out-of-phase barotropic mode with that produced by the easterly VS and damps the local negative barotropic responses near the heating (Figs. 4 and 13a), the barotropic responses away from the heating are enhanced because the PBL will enhance the responses in the upper level (Figs. 4 and 13a), where the prevailing mean westerly winds are favorable for the teleconnection. An elevated heat forcing can enhance the barotropic and the upper-level

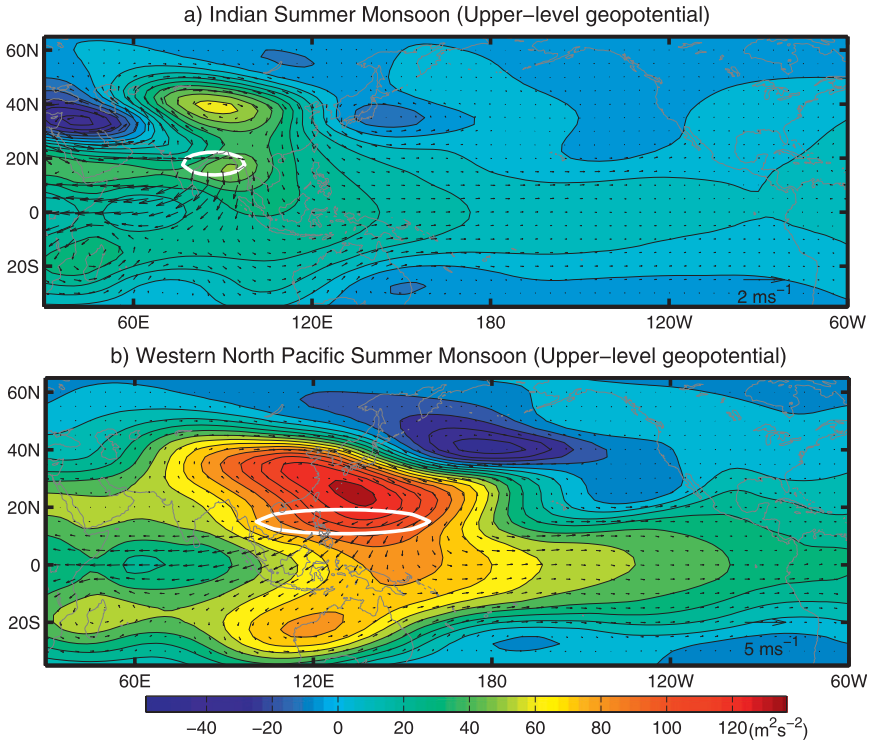

FIG. 12. As in Fig. 8, but without the mean meridional winds.

perturbations, as well as the global teleconnection of the ASM (Fig. 13b). Because the higher heating tends to bring more energy to the upper troposphere, where the energy can propagate in the prevailing mean westerly winds, the VHD is important for modifying the teleconnection of the ASM.

Although the ASM can have global teleconnections, its global responses are relatively weak compared to the

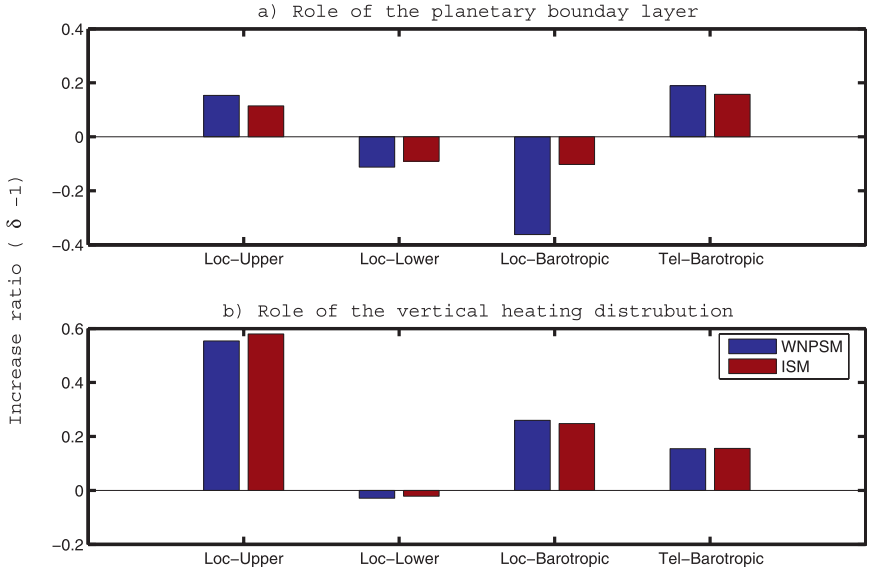

FIG. 13. Role of the (a) PBL and (b) VHD. The increase ratios $\delta - 1$, associated with (a) the sensitivity experiment with a deep PBL pressure depth of 150 hPa and (b) the sensitivity experiment with a high heating at 400 hPa, are drawn for the local (Loc) upper-level, lower-level, and barotropic responses, as well as for the teleconnection (Tel) barotropic responses.

winter teleconnections. Meanwhile, the role of the PBL in modulating the winter teleconnections may be different and needs further work.

Acknowledgments. The authors thank Dr. Zhuo Wang at University of Illinois at Urbana–Champaign for developing an earlier version of the intermediate teleconnection model. This study was supported by Climate Dynamics Program of the National Science Foundation under award AGS-1005599 and by the APEC climate center. Additional support was provided by the Japan Agency for Marine-Earth Science and Technology (JAMSTEC) through their sponsorship of research activities at the International Pacific Research Center.

APPENDIX A

Two-Level Model for the Free Troposphere

The low-frequency motions in the free troposphere satisfy the following linearized primitive equations in a spherical p coordinate:

$$\begin{aligned}
&\partial_t u + (r\cos\psi)^{-1}(Uu_\lambda + uU_\lambda + \phi_\lambda)\\
&\quad + r^{-1}(Vu_\psi + vU_\psi) - 2\Omega v\sin\psi = -\varepsilon u + K\nabla^2 u,\\
&\partial_t v + (r\cos\psi)^{-1}(Uv_\lambda + uV_\lambda)\\
&\quad + r^{-1}(Vv_\psi + vV_\psi + \phi_\psi) + 2\Omega u\sin\psi = -\varepsilon v + K\nabla^2 v,\\
&\qquad (r\cos\psi)^{-1}u_\lambda + r^{-1}v_\psi + \omega_p = 0,\\
&\quad T_t + (r\cos\psi)^{-1}UT_\lambda + r^{-1}VT_\psi - R^{-1}PS(p)\omega\\
&\qquad = C_p^{-1}Q - \mu T + K\nabla^2 T,\\
&\qquad\qquad p\phi_p = -RT,
\end{aligned} \tag{A1}$$

where ψ and λ are the latitude and longitude; U and V the mean zonal and meridional winds; u, v, ω, ϕ, and T the zonal and meridional wind, vertical pressure velocity, geopotential, and temperature perturbations; ε and μ the Rayleigh friction and Newtonian cooling coefficients, respectively, and r the averaged radius of Earth. Because the equatorial region has much precipitation and then strong cumulus friction (Lin et al. 2008), ε is assumed to be damped poleward from ε_e with an e-folding scale of 15°. Also, K is the horizontal momentum or thermal diffusion coefficient, $S(p)$ the dry static stability parameter, R the gas constant of air, C_p the specific heat at constant pressure, p the pressure, and Q the diabatic heating.

The model structure is shown in Fig. A1, where p_m is the height where the monsoon heating occurs. The upper-level depth Δp_1, lower-level depth Δp_2, and PBL depth Δp_b all can vary to study the role of the vertical heating distribution (VHD) and PBL. A two-level model can be established by writing the momentum and continuity equations at the upper- and lower-tropospheric level of p_1 and p_2:

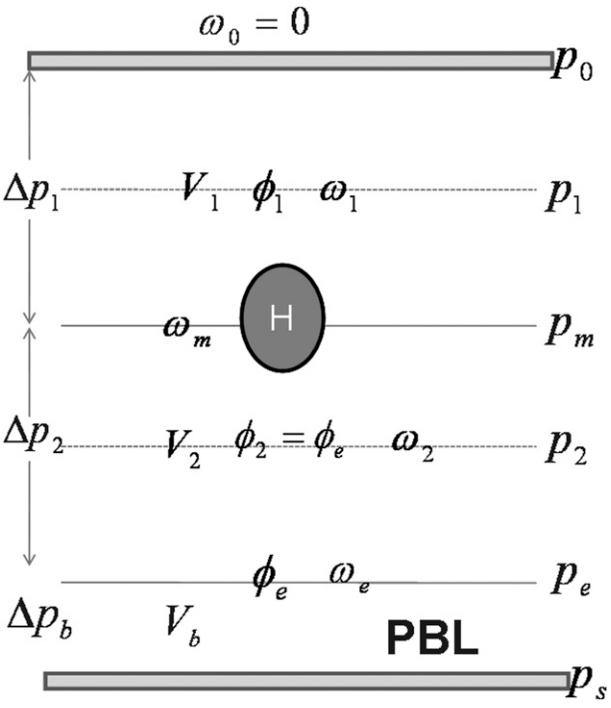

FIG. A1. Schematic vertical structure of the intermediate model, which consists of a two-level troposphere and a barotropic PBL. The letter H represents the monsoon heating.

$$\begin{aligned}
&\partial_t u_j + (r\cos\psi)^{-1}(U_j u_{j\lambda} + u_j U_{j\lambda} + \phi_{j\lambda})\\
&\quad + r^{-1}(V_j u_{j\psi} + v_j U_{j\psi}) - 2\Omega v_j\sin\psi = -\varepsilon u_j + K\nabla^2 u_j,\\
&\partial_t v_j + (r\cos\psi)^{-1}(U_j v_{j\lambda} + u_j V_{j\lambda})\\
&\quad + r^{-1}(V_j v_{j\psi} + v_j V_{j\psi} + \phi_{j\psi}) + 2\Omega u_j\sin\psi = -\varepsilon v_j + K\nabla^2 v_j,\\
&\qquad (r\cos\psi)^{-1}u_{1\lambda} + r^{-1}v_{1\psi} - \Delta p_1^{-1}(\omega_0 - \omega) = 0,\\
&\qquad (r\cos\psi)^{-1}u_{2\lambda} + r^{-1}v_{2\psi} - \Delta p_2^{-1}(\omega - \omega_e) = 0,
\end{aligned} \tag{A2}$$

where the subscript j denotes the upper ($j = 1$) or lower ($j = 2$) level, respectively. A rigid lid is assumed at the tropopause (i.e., $\omega_0 = 0$); ω and ω_e are the vertical pressure velocity at the middle troposphere and the top of the PBL, respectively. The thermodynamic and hydrostatic equations at the midtropospheric level p_m are

$$T_t + (r\cos\psi)^{-1}UT_\lambda + r^{-1}VT_\psi - R^{-1}PS(p)\omega = C_p^{-1}Q - \mu T + K\nabla^2 T,$$
$$(\Delta p_2 + \Delta p_1)^{-1}(\Delta p_2\phi_2 - \Delta p_1\phi_1) = -p_m^{-1}RT. \quad \text{(A3)}$$

In this two-level model, for any variable A, the baroclinic (minus-sign subscript) or barotropic (plus-sign subscript) component can be calculated as

$$A_- = (\Delta p_2 + \Delta p_1)^{-1}(A_2\Delta p_2 - A_1\Delta p_1),$$
$$A_+ = (\Delta p_2 + \Delta p_1)^{-1}(A_2\Delta p_2 + A_1\Delta p_1). \quad \text{(A4)}$$

APPENDIX B

PBL Equations

To determine the geopotential anomalies in Eq. (A1), a stationary barotropic PBL model is implemented into the two-level model. The effects of the PBL mean flows are negligible (Wang 2000), and the PBL equations take the forms of

$$-2\Omega v_b\sin\psi = -(r\cos\psi)^{-1}\phi_{e\lambda} - E_x u_b,$$
$$2\Omega u_b\sin\psi = -r^{-1}\phi_{e\psi} - E_y v_b,$$
$$\omega_e = \Delta p_b[(r\cos\psi)^{-1}u_{b\lambda} + r^{-1}v_{b\psi}], \quad \text{(B1)}$$

where the subscript b denotes the PBL component. Also, $p_s = 1000$ hPa is the pressure on the model surface; E_λ and E_ψ are the Rayleigh friction coefficients in the zonal and meridional directions, respectively. Diagnostic studies using observed monthly mean surface pressure and winds indicated that the Rayleigh friction coefficients should be anisotropic: E_ψ is generally 2 or 3 times as large as E_λ (Deser 1993; Wang and Li 1994). Here we use $E_\psi = 2E_\lambda$.

The Ekman pumping can be obtained from Eq. (B1), which is written as

$$\omega_e = [D_1(r\cos\psi)^{-2}\partial_{\lambda\lambda} + D_2(r\cos\psi)^{-1}\partial_\lambda + D_3 r^{-2}\partial_{\psi\psi} + D_4 r^{-1}\partial_\psi]\phi_e, \quad \text{(B2)}$$

where the coefficients are

$$\{D_1, D_2, D_3, D_4\} = \Delta p_b(E_\lambda E_\psi + f^2)^{-1} \times \{-E_\psi, f_\psi - 2(E_\lambda E_\psi + f^2)^{-1}f^2 f_\psi - r^{-1}f\tan\psi, -E_\lambda, 2(E_\lambda E_\psi + f^2)^{-1}E_\lambda f f_\psi + r^{-1}E_\lambda\tan\psi\}. \quad \text{(B3)}$$

The Coriolis parameter $f = 2\Omega\sin\psi$ and its meridional variation $f_\psi = 2r^{-1}\Omega\cos\psi$. Because of the mass conservation in a vertical column, ω_e is related to the free-tropospheric convergence, that is,

$$\omega_e = -\sum_{j=1}^{2}\Delta p_j[(r\cos\psi)^{-1}u_{j\lambda} + r^{-1}v_{j\psi}]. \quad \text{(B4)}$$

Then Eqs. (B2) and (B4) compose an elliptic equation with respect to ϕ_e.

REFERENCES

Branstator, G., 1983: Horizontal energy propagation in a barotropic atmosphere with meridional and zonal structure. *J. Atmos. Sci.,* **40,** 1689–1708.

——, 2002: Circumglobal teleconnections, the jet stream waveguide, and the North Atlantic Oscillation. *J. Climate,* **15,** 1893–1910.

Davey, M. K., and A. E. Gill, 1987: Experiments on tropical circulation with a simple moist model. *Quart. J. Roy. Meteor. Soc.,* **113,** 1237–1269.

Deser, C., 1993: Diagnosis of the surface momentum balance over the tropical Pacific Ocean. *J. Climate,* **6,** 64–74.

Ding, Q., and B. Wang, 2005: Circumglobal teleconnection in the Northern Hemisphere summer. *J. Climate,* **18,** 3483–3505.

——, and ——, 2007: Intraseasonal teleconnection between the summer Eurasian wave train and the Indian monsoon. *J. Climate,* **20,** 3751–3767.

Fulton, S. R., and W. H. Schubert, 1985: Vertical normal mode transforms: Theory and application. *Mon. Wea. Rev.,* **113,** 647–658.

Geisler, J. E., 1981: A linear model of the Walker circulation. *J. Atmos. Sci.,* **38,** 1390–1400.

——, and D. E. Stevens, 1982: On the vertical structure of damped steady circulation in the tropics. *Quart. J. Roy. Meteor. Soc.,* **108,** 87–93.

Gill, A. E., 1980: Some simple solutions for heat-induced tropical circulation. *Quart. J. Roy. Meteor. Soc.,* **106,** 447–462.

Hoskins, B. J., and D. J. Karoly, 1981: The steady linear response of a spherical atmosphere to thermal and orographic forcing. *J. Atmos. Sci.,* **38,** 1179–1196.

——, and T. Ambrizzi, 1993: Rossby wave propagation on a realistic longitudinally varying flow. *J. Atmos. Sci.,* **50,** 1661–1671.

——, and M. J. Rodwell, 1995: A model of the Asian summer monsoon. Part I: The global scale. *J. Atmos. Sci.,* **52,** 1329–1340.

Kalnay, E., and Coauthors, 1996: The NCEP/NCAR 40-Year Reanalysis Project. *Bull. Amer. Meteor. Soc.,* **77,** 437–471.

Kasahara, A., and P. L. da Silva Dias, 1986: Response of planetary waves to stationary tropical heating in a global atmosphere with meridional and vertical shear. *J. Atmos. Sci.,* **43,** 1893–1911.

Kripalani, R. H., A. Kulkarni, and S. V. Singh, 1997: Association of the Indian summer monsoon with the Northern Hemisphere mid-latitude circulation. *Int. J. Climatol.,* **17,** 1055–1067.

Langer, R. E., 1960: *Boundary Problems in Differential Equations*. University of Wisconsin Press, 324 pp.

Lee, S.-K., C. Wang, and B. E. Mapes, 2009: A simple atmospheric model of the local and teleconnection responses to tropical heating anomalies. *J. Climate,* **22,** 272–284.

Lim, H., and C.-P. Chang, 1983: Dynamics of teleconnections and Walker circulations forced by equatorial heating. *J. Atmos. Sci.,* **40,** 1897–1915.

——, and ——, 1986: Generation of internal-and external-mode motions from internal heating: Effects of vertical shear and damping. *J. Atmos. Sci.,* **43,** 948–960.

Lin, H., 2009: Global extratropical response to diabatic heating variability of the Asian summer monsoon. *J. Atmos. Sci.,* **66,** 2697–2712.

Lin, J.-L., B. E. Mapes, and W. Han, 2008: What are the sources of mechanical damping in Matsuno–Gill-type models? *J. Climate,* **21,** 165–179.

Longuet-Higgins, M. S., 1964: Planetary waves on a rotating sphere. *Proc. Roy. Soc. London,* **279A,** 446–473.

Majda, A., and J. A. Biello, 2003: The nonlinear interaction of barotropic and equatorial baroclinic Rossby waves. *J. Atmos. Sci.,* **60,** 1809–1821.

Matsuno, T., 1966: Quasi-geostrophic motions in the equatorial area. *J. Meteor. Soc. Japan,* **44,** 25–42.

Michaels, P. J., 2005: *Shattered Consensus: The True State of Global Warming.* Rowman and Littlefield, 174 pp.

Nitta, T., 1987: Convective activities in the tropical western Pacific and their impacts on the Northern Hemisphere summer circulation. *J. Meteor. Soc. Japan,* **65,** 373–390.

——, 1989: Global features of the Pacific–Japan oscillation. *Meteor. Atmos. Phys.,* **41,** 5–12.

Rodwell, M. J., and B. J. Hoskins, 1996: Monsoons and the dynamics of deserts. *Quart. J. Roy. Meteor. Soc.,* **122,** 1385–1404.

——, and ——, 2001: Subtropical anticyclones and summer monsoons. *J. Climate,* **14,** 3192–3211.

Sardeshmukh, P., and B. Hoskins, 1988: The generation of global rotational flow by steady idealized tropical divergence. *J. Atmos. Sci.,* **45,** 1228–1251.

Silva Dias, P. L., W. H. Schubert, and M. DeMaria, 1983: Large-scale response of the tropical atmosphere to transient convection. *J. Atmos. Sci.,* **40,** 2689–2707.

Ting, M., and P. D. Sardeshmukh, 1993: Factors determining the extratropical response to equatorial diabatic heating anomalies. *J. Atmos. Sci.,* **50,** 907–918.

Wang, B., and T. Li, 1994: Convective interaction with boundary-layer dynamics in the development of a tropical intraseasonal system. *J. Atmos. Sci.,* **51,** 1386–1400.

——, and X. Xie, 1996: Low-frequency equatorial waves in vertically sheared zonal flow. Part I: Stable waves. *J. Atmos. Sci.,* **53,** 449–467.

——, and ——, 1997: A model for the boreal summer intraseasonal oscillation. *J. Atmos. Sci.,* **54,** 72–86.

——, and Z. Fan, 1999: Choice of South Asian summer monsoon indices. *Bull. Amer. Meteor. Soc.,* **80,** 629–638.

——, R. Wu, and K.-M. Lau, 2001: Interannual variability of the Asian summer monsoon: Contrasts between the Indian and the western North Pacific–East Asian monsoons. *J. Climate,* **14,** 4073–4090.

Wang, Z., 2000: The response of the tropical atmosphere to diabatic heating: Effects of the boundary layer and mean flows. M.S. thesis, Dept. of Meteorology, University of Hawaii at Manoa, 51 pp.

Webster, P. J., 1981: Mechanisms determining the atmospheric response to sea surface temperature anomalies. *J. Atmos. Sci.,* **38,** 554–571.

——, 1982: Seasonality in the local and remote atmospheric response to sea surface temperature anomalies. *J. Atmos. Sci.,* **39,** 41–52.

Wu, Z., E. S. Sarachik, and D. S. Battisti, 2000: Vertical structure of convective heating and the three-dimensional structure of the forced circulation on an equatorial beta plane. *J. Atmos. Sci.,* **57,** 2169–2187.

Zhang, Z., and T. N. Krishnamurti, 1996: A generalization of Gill's heat-induced tropical circulation. *J. Atmos. Sci.,* **53,** 1045–1052.